LA-UR- 92-2913

Title: EQUILIBRIUM CHARGE STATE DISTRIBUTIONS OF 1-30 KEV ATOMIC PROJECTILES TRANSITING THIN CARBON FOILS

LA-UR--92-2913

DE93 000792

Author(s): H.O. Funsten, B.L. Barraclough, D.J. McComas

Submitted to: Eighth International Conference on Ion Beam Modification of Materials, Heidelberg, Germany 7-11 SEPT 1992

Los Alamos
NATIONAL LABORATORY

Equilibrium Charge State Distributions of Medium Energy Atomic Projectiles Transiting Thin Carbon Foils

H.O. Funsten, B.L. Barraclough, and D.J. McComas
MS-D438, Los Alamos National Laboratory
Los Alamos, NM 87545, USA

ABSTRACT

We have investigated the exit charge state distributions of 1-30 keV H, He, C, N, O, Ne, and Ar ions that transit thin carbon foils. In this velocity regime which is less than the Bohr velocity, the dominant charge states are neutrals and singly positive ions. Therefore, the charge state distributions are dependent primarily on electron loss by neutrals with an associated electron loss cross section σ_l and electron capture by singly ionized species with an associated electron capture cross section σ_c. Using empirical charge state distributions, the ratio σ_l/σ_c is shown to have a quadratic dependence on the projectile velocity and is fit to the equation $A(E_l-E_p)/m$ where E_l is the exit projectile energy, m is its mass, and A and E_p are constants. A pronounced shell effect is observed: the constant A is dependent on the principle quantum number of the projectile, and E_p depends on the number of projectile valence electrons.

1. INTRODUCTION

Electron capture and loss by projectiles with a velocity less than the Bohr velocity v_0 is of considerable interest as a fundamental atomic interaction phenomena that can be applied to energy loss of atomic projectiles transiting solids [1,2] and beam-foil experiments. A considerable amount of work has been performed on charge state distributions and charge exchange cross sections for energetic ($v >> v_0$) projectiles transmitted through gaseous and solid targets [3,4] and slow ($v << v_0$) projectiles backscattered from solid surfaces [5-7]. A salient reason for investigating charge exchange in these velocity regimes is the theoretical simplicity. For projectile velocities significantly greater than the velocity of orbiting electrons, the interaction between the projectile and each encountered target atom can be treated independently and the electrons are assumed to be stationary. Alternately, the interaction of low velocity projectiles with target atoms can be treated adiabatically.

Between the adiabatic and stationary treatments lies a relatively uninvestigated realm of velocities near the Fermi velocity of the target electrons where theoretical treatment of charge exchange is complicated. In this paper, we present equilibrium charge state distributions for a variety of 1-36 keV ions incident on 0.5 $\mu g/cm^2$ carbon foils.

In the velocity regime used in this study, the fraction of the incident beam that exits the foil in the charge state +2 was unmeasurable (< 0.1%) except for a trace fraction (< 1%) in N and He. Therefore, we ignore the possibility of $q = +2$ exit charge states. Furthermore, if we exclude the possibility of double electron loss or capture, then the fraction f^+ of the beam in the $q = +1$ state is a function of the populations of the $q = 0$ and $q = +1$ states only and is independent of the population of the $q = -1$ charge state. The variation of the fraction of the beam in charge state $q = +1$ with penetration distance x into the foil can be described as

$$\frac{1}{n}\frac{df^+(x)}{dx} = \sigma_l f^0(x) - \sigma_c f^+(x) \qquad (1)$$

where n is the atomic density of the foil, f^0 is the fraction of neutrals, σ_l is the electron loss cross section for the transition $q = 0$ to $q = +1$, and σ_c is the electron capture cross section for the transition $q = +1$ to $q = 0$. However, the simplicity of this equation is exaggerated since f^+ and f^0 each include a large number of excitation levels. In solids these excited states play a significant role in charge exchange: excitation lifetimes that are longer than the time between collisions and multiple projectile excitations result in a higher mean charge of the exiting beam [4].

Charge state equilibrium is rapidly obtained; in fact, studies have shown that equilibrium occurs within a penetration distance of 3 Å [3,7]. If the foil thickness is greater than the penetration distance to reach charge equilibrium, then $df^+(x)/dx = 0$ at the exit surface of the foil. Therefore, for charge state equilibrium eq. 1 simplifies to

$$\frac{f^+}{f^0} = \frac{\sigma_l}{\sigma_c} \quad . \tag{2}$$

Equation 2 provides direct insight into fundamental physical constants governing charge exchange using empirical charge state distribution results.

For hydrogen, a possible concern with this approach is the prevention of bound electron states in a metal due to electron screening of the proton [8,9] and invalidates eq. 1. However, if we assume carbon is graphite, then the conduction electron concentration is four orders of magnitude less than a metal and screening is negligible [10]. In addition to theoretical arguments that question the validity of this type of screening [11,12], empirical evidence of neutralization within the solid has been observed for H and other projectiles backscattered from metals [13,14]. Consequently, in this study we assume the existence of neutral projectiles with bound electron states in the foil.

2. EXPERIMENTAL APPARATUS

Fig. 1 depicts the experimental apparatus used to obtain the exit charge state distributions and is similar to the apparatus used by Burgi *et al.* [15]. Positive ions were generated using a duoplasmatron ion source, accelerated to an energy of 1-30 keV, and magnetically mass analyzed. The ions were incident on a 1 mm round aperture located directly in front of the foil. Located 30 mm behind the foil was a 0.35x25 mm slit. Projectiles that passed through the slit were charge-separated using electrostatic deflection plates. The separated charge state distributions were detected and imaged using an imaging microchannel plate (IMCP) detector and position computer. Charge state fractions were derived by summing all counts in each charge state distribution and dividing by the total number of counts in all distributions. The pressure of the target chamber was typically $3x10^{-8}$ torr.

The detection efficiency is dependent on the incident species and energy. Since only one incident ion species and energy were examined at a time and the exit charge state is independent of the energy loss of the projectile in the foil, charge state distributions could be directly compared. Typically, the counting rate of the detector was 2-3 kHz and the total collection time was five minutes.

Carbon foils with a nominal thickness of 0.5 $\mu g/cm^2$ were obtained from Arizona Carbon Foil and were mounted on 333 line-per-inch nickel grid. The foil surfaces likely are composed of various chemisorbed species due to their prolonged exposure to air, so the charge state distributions derived using these foils are characteristic of "practical" foils whose surfaces have been contaminated by chemisorbed species [10]. The foil thickness is approximately 44 Å based on comparison of the scattering halfwidth of hydrogen with the Meyer theory of small-angle scattering [16]. Since the foil thickness is much greater than the penetration depth characteristic of charge state equilibrium, the exit beam is in charge state equilibration.

Ultra-thin foils used in this study can have pinholes that allow the incident ion beam to pass without charge modification [17]. This results in a localized high-flux region on the IMCP detector in the charge state distribution equal in charge to the incident ion beam. Since this high-flux region is readily observed using the imaging capabilities of the IMCP detector, it can be avoided during subsequent data analysis.

3. RESULTS

Fig. 2 depicts the equilibrium fraction of an incident beam that exits the foil in charge state q = +1 as a function of the incident energy E_0 for incident ion species of (a) H and He and (b) C, N, O, Ne, and Ar. Only positive and neutral exit species were observed from He, N, Ne, and Ar so the neutral fraction is simply $1 - f^+$ where f^+ is the positive ion fraction. Negative ions were observed in the exit charge state distributions for the electronegative species H, C, and O. Since we assume multiple electron capture or loss is negligible for the derivation of eq. 2, we focus only on the positive and neutral charge state fractions. Except for hydrogen, the projectile velocities spanned by the data are all below the Bohr velocity which corresponds to an energy of 25 keV/amu.

The final charge state distribution of the beam of projectiles is established near the exit surface of the foil at the exit velocity of the projectiles. Due to energy loss in the foil, the exit energy E_0 is less than the incident energy E_0 and therefore was calculated using the following method. The stopping powers of projectiles transiting carbon were obtained using the TRIM90 code [18]. To derive the energy loss of projectiles in the foil, the stopping power was integrated over the 44 Å foil thickness. Since the stopping power is slow varying over the energy range investigated in this study, the energy loss increases linearly with increasing incident energy E_0. Based on linear least squares fit of the energy loss to E_0 for a 44 Å carbon foil, an expression for the exit energy E_1 as a function of E_0 was derived and is listed in Table 1.

Fig. 5 depicts the ratio σ_l/σ_c (which equals f^+/f^0 according to eq. 2) as a function of E_l/m where m is the projectile mass in amu. The data clearly shows a linear dependence of σ_l/σ_c on E_l/m or, equivalently, the square of the projectile exit velocity, v_l^2. A linear least-squares fit to the equation

$$\frac{\sigma_l}{\sigma_c} = \frac{A\,(E_F - E_T)}{m} \tag{3}$$

was performed on the data, and the results are tabulated in Table 2. The factor A reflects the magnitude of the enhancement of σ_l relative to σ_c due to the exit velocity.

The threshold energy E_T is the extrapolated minimum energy required for the existence of positive exit charge states. Qualitatively, E_T describes the energy-independent enhancement of σ_l relative to σ_c and should depend on the projectile and foil properties. Since one foil was used throughout the entire experiment, variations in E_T can be attributed to different projectile properties. For a positive E_T, positive ions exiting the foil will be observed only if E_F is greater than E_T. A negative value of E_T infers that positive ions will be observed exiting the foil at any energy.

The derived values for A and E_T exhibit a striking correlation with the projectile shell structure. The constant A can be separated into three distinct groups that correspond closely to the principle quantum number n of the projectile: for $n = 1$ (H and He), $A \approx 0.021$; for $n = 2$ (C, N, O, and Ne) $A \approx 0.085$; and for $n = 3$ (Ar), $A = 0.4$. Apparently, electron loss is facilitated by increased electron screening associated with larger quantum numbers.

A more subtle effect is apparent within a principle quantum level: A decreases (i.e., σ_l is enhanced relative to σ_c) with increasing atomic number. The exception is carbon, which involves symmetrical resonance reactions with carbon atoms in the foil that may lead to enhanced electron capture.

Within a principle quantum number, a more negative value of E_T indicates an enhancement of electron loss relative to electron capture. This effect is clearly observed in both Fig. 3 and Table 2 which show that the σ_l/σ_c enhancement is larger for projectiles with fewer valence electrons. A general anti-correlation between E_T and the ionization potential is noted, although this would predict a larger value of E_T for oxygen relative to nitrogen which is not observed in the data.

At higher energies, the velocity dependence of σ_l/σ_c sharply increases. The relationship between f^+/f^0 and σ_l/σ_c described in eq. 2 has been previously performed using hydrogen at energies greater than 20 keV on a variety of foils [19,20]. Their results show that σ_l/σ_c varies with the exit velocity as approximately v_l^2 at 25 keV to v_l^{10} at 400 keV. These values are consistent with theoretical predictions by Bohr [1].

In Fig. 3, the charge state distributions for H and He differ by a factor of 2. Previous results of backscattered H and He that penetrate the solid show nearly identical charge state distributions at

velocities higher [14] and lower [13] than those used in this study. This apparently results for screening of He in metal targets resulting in at least one continuously bound electron so that He behaves identically to H. The large variation between H and He observed in this study show that He^+ cannot be treated as a proton. If we ignore the possibility of He^{+2} in the foil (based on the minute fraction (< 1%) of He^{+2} observed in the exit charge state distribution), then He always then has at least one bound electron while in the foil. Therefore, the variation in σ_l/σ_c between H and He must result from multiple excitations of He during charge exchange interactions.

SUMMARY

Based on the exit charge state distributions of various atomic projectiles over an energy range of 1-30 keV, the ratio of the electron loss to capture cross sections show a quadratic dependence on the exit projectile velocity. The variation of this ratio with energy is dependent on the projectile principle quantum number. Velocity-dependent enhancement of σ_l relative to σ_c due to projectile shell effects is observed for both larger principle quantum numbers and, for a given quantum number, a smaller atomic number. Velocity-independent enhancement of σ_l relative to σ_c is observed for projectiles with fewer outer-shell electrons.

Based on the small fraction of exiting He^{+2} observed in this study, He likely carries at least one bound electron in the foil. Therefore, the difference in σ_l/σ_c between H and He projectiles suggests that multiple excited states are involved in He charge exchange interactions and He cannot be treated as a proton.

ACKNOWLEDGEMENTS: This work was performed under the auspices of the United States Department of Energy. The authors gratefully acknowledge the contributions of J.R. Baldanado, and D.T. Everett.

REFERENCES

[1] N. Bohr, 1948, Kgl. Danske Videnskab. Selskab, Mat.-Fys. Medd. **28**, No. 7.

[2] B.S. Yarlagadda, J.E. Robinson,and W. Brandt, Phys. Rev. **B17** (1978) 3473.

[3] H.D. Betz, in Applied Atomic Collision Physics, Vol. 4, ed. S. Datz (Academic, New York, 1983) 1-42.

[4] H.D. Betz, Rev. Mod. Phys. **44** (465) 1973.

[5] W. Heiland, in Interaction of Charged Particles with Solids and Surfaces, eds. A. Gras-Marti, H.M. Urbassek, N.R. Arista, and F. Flores (Plenum, New York, 1991) 253-307.

[6] S.R. Kasi, H. Kang, C.S. Sass, and J.W. Rabalais, Surf. Sci. Repts. **10** (1989) 1.

[7] W. Eckstein, in Inelastic Particle-Surface Collisions, eds. E. Taglauer and W. Heiland (Springer, New York, 1981) 157-183.

[8] B.A. Trubnikov and Y.N. Yavlinskii, Sov. Phys. JETP **25** (1967) 1089.

[9] W. Brandt, in Atomic Collisions in Solids, Vol. 1, eds. S. Datz, B.R. Appleton, and C.D. Moak (Plenum, New York, 1975) 261-288.

[10] K.H. Berkner, I. Bornstein, R.V. Pyle, and J.W. Stearns, Phys. Rev. **A6** (1972) 278.

[11] F. Guinea, F. Flores, and P.M. Echenique, Phys. Rev. **B25** (1982) 6109.

[12] M.C. Cross, in Inelastic Ion-Surface Collisions, eds. N.H. Tolk, J.C. Tully, W. Heiland, and C.W. White (Academic, New York, 1977) 253-281.

[13] R.S. Bhattacharya, W. Eckstein, and H. Verbeek, Surf. Sci. **93** (1980) 563.

[14] T.M. Buck, in Inelastic Ion-Surface Collisions, eds. N.H. Tolk, J.C. Tully, W. Heiland, and C.W. White (Academic, New York, 1977) 253-281.

[15] A. Burgi, M. Oetliker, P. Bochsler, J. Geiss, and M.A. Coplan, J. Appl. Phys. **68** (1990) 2547.

[16] H.O. Funsten, D.J. McComas, and B.L. Barraclough, SPIE Vol. 1744 (1992) 62.

[17] H.O. Funsten, D.J. McComas, and B.L. Barraclough, Nucl. Instrum. Meth. **B66** (1992) 470.

[18] J.F. Ziegler, TRIM 90 Computer Code, IBM-Research, Yorktown, NY, 1990.

[19] T. Hall, Phys. Rev. **79** (1950) 504.

[20] J.A. Phillips, Phys. Rev. **97** (1955)404.

FIGURE CAPTIONS

Fig. 1. Experimental apparatus.

Fig. 2. The fraction of atomic beams exiting as ions with charge state q = +1 is depicted as a function of incident ion energy E_o.

Fig. 3. The fraction f^+/f^o, which equals σ_l/σ_c according to equation 2, is plotted as a function of the calculated exit energy of the projectiles for (a) H and He and (b) C, N, O, and Ar. The data clearly shows a linear dependence of σ_l/σ_c on the square of the projectile's exit velocity.

Table 1. Final projectile energy E_F calculated using tabulated stopping powers [TRIM90].

Projectile	$E_F = c_1 E_0 - c_2$, 1 keV < E_0 < 30 keV	
	c_1	c_2
H	0.991	0.333
He	0.984	0.310
C	0.990	1.461
N	0.988	1.756
O	0.989	1.974
Ne	0.992	2.403
Ar	0.957	4.018

Table 2. Least Squares Fit Parameters for $\sigma_I/\sigma_c = A(E_I-E_T)/m$.

Element	n	A	E_T(keV)
H	1	0.0264	-1.77
He	1	0.0169	5.25
C	2	0.0864	-7.61
N	2	0.0917	-5.13
O	2	0.0840	2.32
Ne	2	0.0745	4.32
Ar	3	0.423	6.39

Figure 1.

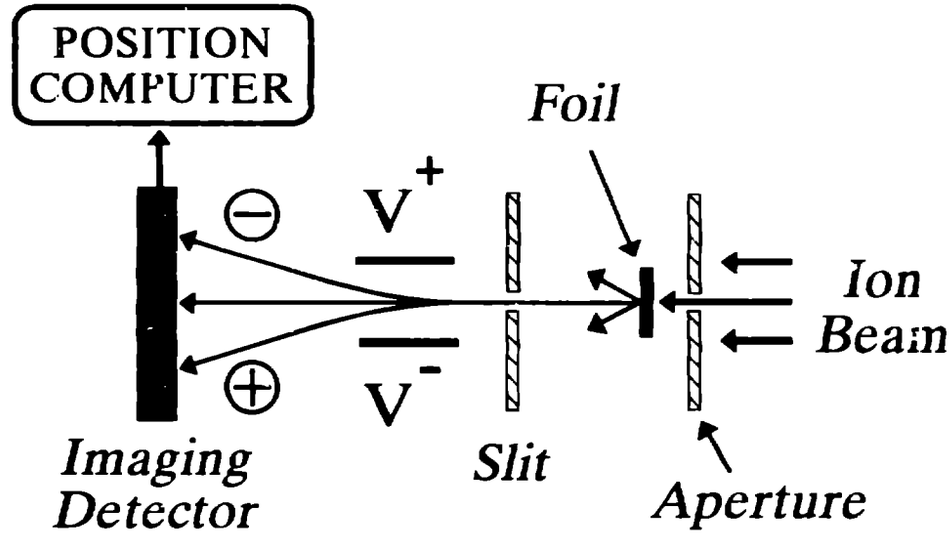
POSITION COMPUTER
Foil
V+
V-
Ion Beam
Imaging Detector
Slit
Aperture

Figure 2.

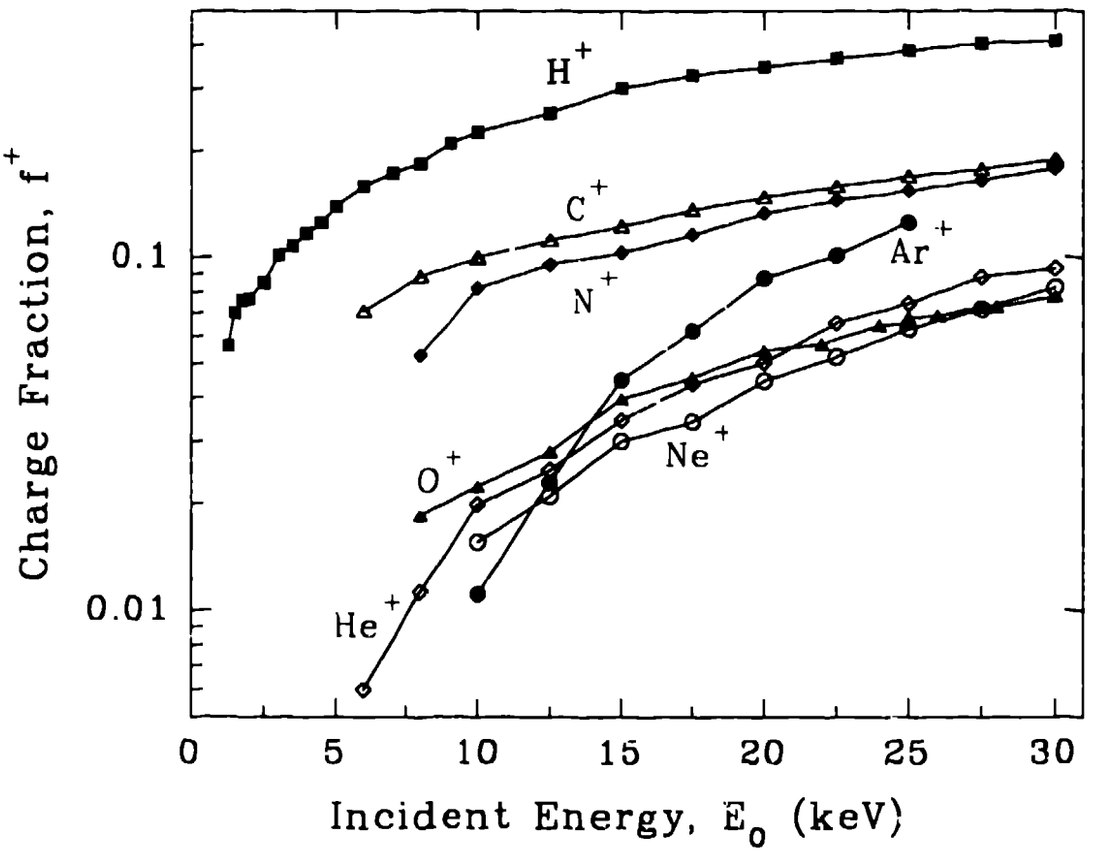
Charge Fraction, f^+
0.1
0.01
0
5
10
15
20
25
30
Incident Energy, E_0 (keV)
H^+
C^+
N^+
Ar^+
O^+
Ne^+
He^+

FIGURE 3.

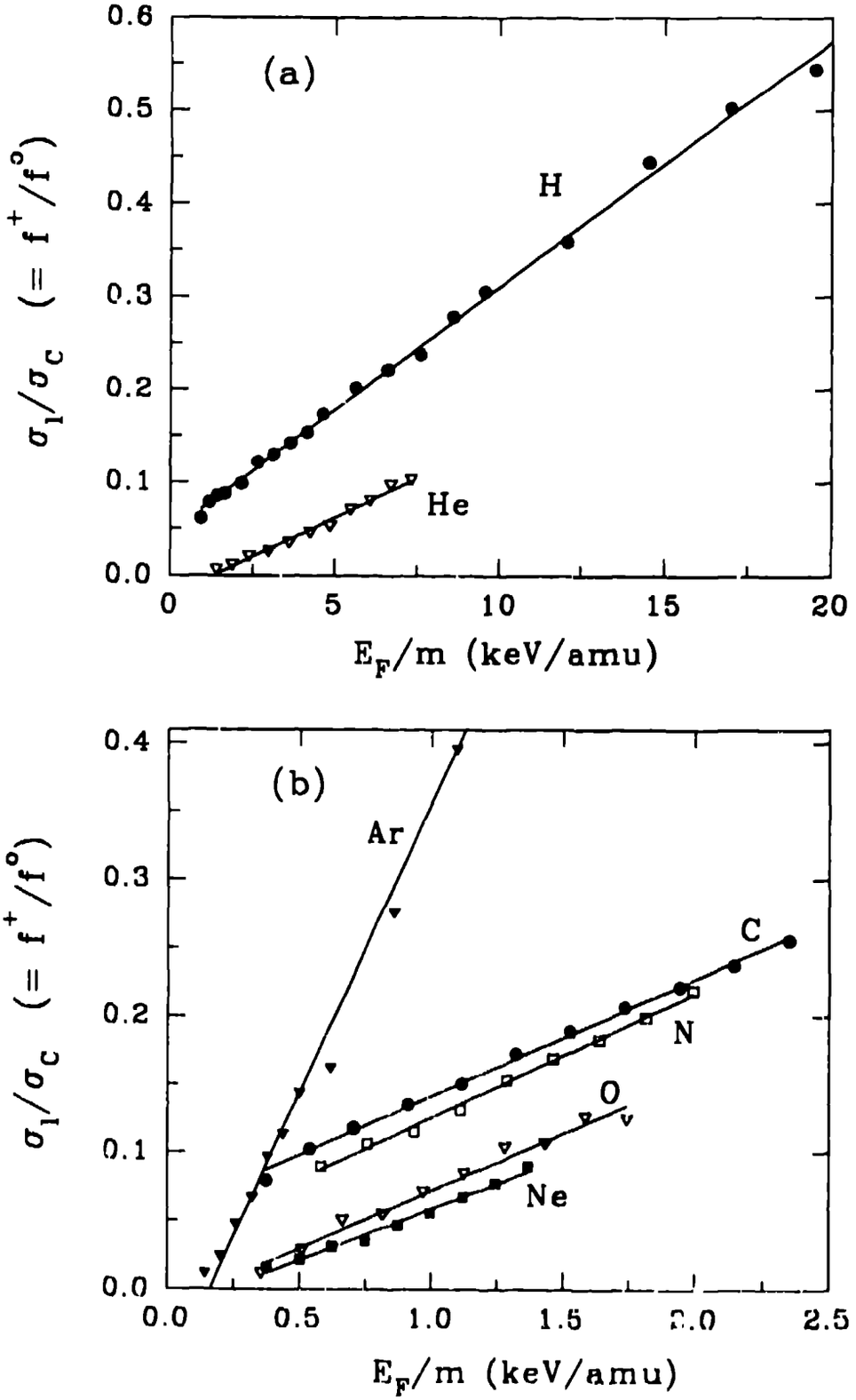
(a)
H
He
σ_1/σ_c (= f^+/f°)
E_F/m (keV/amu)
0.0
0.1
0.2
0.3
0.4
0.5
0.6
0
5
10
15
20
(b)
Ar
C
N
O
Ne
σ_1/σ_c (= f^+/f°)
E_F/m (keV/amu)
0.0
0.1
0.2
0.3
0.4
0.5
1.0
1.5
2.0
2.5